First Principles Density Functional Study of the Adsorption and Dissociation of Carbonyl Compounds on Magnesium Oxide Nanosurfaces

ARTICLE *in* THE JOURNAL OF PHYSICAL CHEMISTRY B · DECEMBER 2006

Impact Factor: 3.3 · DOI: 10.1021/jp0603536 · Source: PubMed

3 AUTHORS:

Rita Kakkar
University of Delhi
110 PUBLICATIONS **584** CITATIONS
SEE PROFILE

Pramesh N Kapoor
University of Delhi
121 PUBLICATIONS **1,655** CITATIONS
SEE PROFILE

Kenneth Klabunde
Kansas State University
357 PUBLICATIONS **13,808** CITATIONS
SEE PROFILE

First Principles Density Functional Study of the Adsorption and Dissociation of Carbonyl Compounds on Magnesium Oxide Nanosurfaces

Rita Kakkar,*,† Pramesh N. Kapoor,† and Kenneth J. Klabunde‡

Departments of Chemistry, University of Delhi, Delhi-110 007, India, and Kansas State University, Manhattan, Kansas 66506

Received: January 18, 2006; In Final Form: September 29, 2006

The adsorption and dissociation of three carbonyl compounds, formaldehyde, acetaldehyde, and acetone, on the magnesium oxide nanosurface, consisting of four stacked $(MgO)_3$ hexagons, is investigated by first principles density functional theory (DFT). In the case of formaldehyde, strongly chemisorbed species, with carboxylate-like structures, are initially formed. These may subsequently undergo heterolytic cleavage of an aldehyde C—H bond to form formate ions involving a surface oxide ion and a hydride ion adsorbed over the magnesium dication $[(MgH^+)(HCOO^-)]$. For acetaldehyde, besides this reaction leading to the formation of acetate, the methyl hydrogen of the adsorbed species also tends to attach itself to a surface oxide ion, yielding surface hydroxyl ions and adsorbed $[CH_2{=}C(H)OMg]^+$. These results are in accord with our previous experimental and theoretical results. In particular, the shift of the aldehyde C—H vibration band to higher frequency and the appearance of OH bands in the infrared spectrum are clearly accounted for. For acetone, the mechanism is found to be similar, i.e., a methyl hydrogen shift to yield surface enolate. Again, this is in agreement with experimental studies.

I. Introduction

Nanosized metal oxides are highly active for a large number of reactions that are important in both pollution control and chemical synthesis.[1−3] The high activity of small particles may not only be due to the higher proportion of surface sites, but may also be attributed to the larger proportion of lower coordination sites as the crystallite size decreases.[1] In addition, our earlier studies had indicated that the presence of defect sites leads to many more different products depending on the nature of the defect.

Although the catalytic activity of bulk MgO is lower than other more basic solids, such as heavier alkaline earth oxides,[4] its well-known structure makes it a model system for solid state and surface studies due to its simple crystalline structure and ionic bonding. Magnesium oxide crystals are also suitable for mechanistic studies, as they exhibit catalytic activity for hydrogen isotope exchange,[5,6] water-gas shift,[7] oxidative coupling of methane,[8−10] hydrogenation of 1,3-butadiene;[11] and other reactions. It was established more than two decades ago that the catalytic activity of the surface of undoped MgO is determined by a small number of defect sites (steps, kinks, corners, etc.) with surface ions (especially oxygen) having low coordination numbers.[12,13] In particular, dissociative adsorption of hydrogen molecules on pairs of adjacent low-coordinated O^{2-} and Mg^{2+} ions can take place via a heterolytic mechanism,[14−18] resulting in the formation of HO^- and HMg^+ surface groups. Other reactions on the MgO surface which involve a heterolytic cleavage include the dissociative adsorption of methane[19] in which a C—H bond breaks in a similar fashion.

Theoretical and experimental studies have established a qualitative correlation between the chemical properties of the surface Mg—O pairs and their coordination numbers: hydrogen adsorption energy,[20−22] hydrogen desorption temperature,[16−18,23] and vibrational frequencies of the HO^- groups[6,24] decrease in the sequence $Mg_{3c}—O_{3c} > Mg_{4c}—O_{3c} > Mg_{4c}—O_{4c}$, while ionicity[21,22,25,26] and surface exciton energy[27,28] increase in the same order. The explanation of these correlations was based on the observation that surface sites with lower coordination numbers usually have lower Madelung constants. This results in lower band gap and ion charges. Enhanced covalency of the low-coordinated sites in turn favors electron transfer from the bonding σ orbital of the hydrogen molecule to the surface and from the surface to the antibonding σ^* orbital, cleavage of the H—H bond, and formation of stronger O—H and Mg—H bonds.[21,29]

Although bulk MgO has been the subject of several studies cited above, very little information exists about nanosized clusters of MgO. Properties of materials at finite scales of length are often different from those in the bulk. For example, our calculations on small MgO clusters[1] had revealed that there is a significant contribution of covalent bonding in these, compared to that in the bulk, in which the bonding is predominantly ionic with ion charges of almost ±2. It was also found that the geometries are also significantly different from those in the bulk, the Mg—O bond distances decreasing significantly, particularly at the edges. Another feature of our calculations was the prediction that the reactive $(MgO)_{12}$ species is not a cubic bulklike structure, but a nanotube. Even when the initial structure was taken as a bulklike structure, it tended to distort to a nanotube on adsorption of formaldehyde. We shall investigate this aspect further in this paper to see whether this distortion is a requirement for adsorption (as it reduces the coordination number of the surface sites from five to four), or the nanotube is actually more stable than the bulklike structure at this length scale.

In this paper, we also report theoretical studies of the

* Corresponding author. E-mail: rita_kakkar@vsnl.com.
† University of Delhi.
‡ Kansas State University. E-mail: kenjk@pop.ksu.edu.

10.1021/jp0603536 CCC: $33.50
Published on Web 11/23/2006

adsorption and dissociation of small molecules on the nanocluster. The dissociation of volatile organic compounds (VOCs) on nanosized metal oxide surfaces has recently assumed importance after the observation that these particles have the capability to dissociatively adsorb toxic organic pollutants including aldehydes and ketones.[2] VOCs represent a large class of substances that contribute to both indoor and outdoor air pollution. The damaging effects of VOCs are numerous, ranging from minor annoyances such as eye, nose, and throat irritation, headaches, and nausea to serious dangers such as damage to the kidneys, liver, and central nervous system. Long-term exposure to some VOCs such as benzene is known to cause cancer. Improvement of indoor air quality is particularly important, as the people who are constantly exposed to VOCs are also particularly vulnerable: the aged, the infirm, and babies.

In an effort to search for better materials to control environmental pollution and to improve the quality of indoor air, we have attempted here to characterize the modes of dissociation of formaldehyde, acetaldehyde, and acetone on the magnesium oxide nanosurface. We had previously performed density functional calculations[1] on the adsorption of formaldehyde on nanosized MgO. The results showed the following: (1) Formaldehyde chemisorbs onto the Lewis acid−base pair sites on the MgO surface, producing zwitterionic four-membered rings, in which the carbonyl CO bond is considerably weakened. (2) The size of the nanocluster has negligible effect on the adsorption energies. (3) Lower coordination sites are definitely preferred over the surface sites and form stronger bonds with the carbonyl moiety, resulting in the weakening of surface Mg—O bonds. (4) In the case of adsorption at 5-coordinate sites, unless severe reconstruction of the surface occurs, no chemisorption takes place. The reconstruction makes the surface take on a cylindrical shape, reducing the coordination number of the surface Mg and O atoms to four. (5) Adsorption at defect sites yields many new, different products.

The results provide a significant advance to our knowledge of chemistry at nanosurfaces. They provide a rationale for the high activity of these surfaces, since these have a larger proportion of the active low-coordination sites than regular metal oxides, and can easily assume different shapes, producing stronger bonds with the chemisorbed species.

II. Computational Methods

First-principles density functional (DF) calculations were performed using the DMol^3 code[30−33] available from Accelrys Inc. in the Materials Studio 3.2 package. DMol^3 uses numerical functions on an atom centered grid as its atomic basis. These basis sets were constructed specifically for use in DFT calculations. Their high quality minimizes superposition (BSSE) effects, and consequently, dissociation of molecules, for example, is accurately described. The long-range tail of the basis set exhibits correct charge distribution and allows an improved description of molecular polarizabilities.[34] Our calculations employed numerical basis sets of double-ζ quality plus polarization functions (DNP) to describe the valence orbitals of O, C, Mg, and H. DFT semilocal pseudopotentials (DSPP),[35] developed specifically for DMol^3, were used to describe the cores.

Geometry and transition state optimizations, without restrictions, were performed using delocalized internal coordinates.[36] The exchange-correlation contribution to the total electronic energy was treated in a spin-polarized generalized-gradient corrected (GGA) form of the local density approximation (LDA),[37] with the Perdew−Burke−Ernzerhof (PBE) correlation.[38] Density functional calculations at the GGA level are expected to give good prediction for the bonding energies of the carbonyl systems on the oxide surfaces.[37,39,40] Transition states were determined via the LST/QST method implemented in DMol^3. The transition states are automatically refined via the conjugate gradient method.

The charge distributions were estimated using the molecular electrostatic potential fitting approach.[41] Our previous calculations[42] had shown that these are superior to those calculated from the Mulliken treatment, as they are consistent and independent of basis size effects. Free valences and bond orders were calculated using Mayer's procedure.[43]

III. Results

III.1. Adsorption and Dissociation of Formaldehyde. We first considered the adsorption of formaldehyde on the MgO surface. The knowledge of the perturbations and transformations of the C_1 molecules on solid surfaces is necessary for understanding the mechanisms of some heterogeneously catalyzed reactions of relevant industrial interest, such as CO hydrogenations and methanol conversions. Formaldehyde is either the product[44] or an intermediate in methanol oxidation[45] and may also be utilized to produce methyl formate via heterogeneously catalyzed Tischenko disproportionation.[46] Moreover, its adsorbed forms are thought to be key intermediates in methanol dehydrogenation[47] and synthesis,[48] as well as, possibly, in higher alcohol[49] and Fischer−Tropsch syntheses.[50] Several spectroscopic papers have been published concerning the adsorption of formaldehyde on oxide surfaces.[51−55] The formaldehyde molecule has also been the focus of many experimental and theoretical studies due to its importance in the atmosphere, interstellar space, and combustion chemistry. Also, its small size allows ab initio calculations at a high level of theory, as well as trajectory and vibrational transition state studies. It is also a possible carcinogen and is present indoors in large concentrations, as it is emitted from building materials, furniture, some cosmetics, paper products, and permanent-press fabrics including clothing and drapes.

Since our earlier calculations[1] had indicated that the 12-MgO unit cluster is adequate for studying the adsorption of formaldehyde on nanocrystalline MgO, we have taken this model for the present calculations. In any case, we had found that the cluster size has little effect on the calculated adsorption energies. More important are the coordination numbers at the adsorption site. Formaldehyde binds with the carbonyl carbon coordinated with a surface oxygen atom and the carbonyl oxygen with a surface magnesium atom, resulting in a four membered complex. The binding was found to be strong at pairs of MgO 3c sites, at which the Mg—O and O—C bond orders were found to be 0.4 and 0.7, respectively.[1] As a result of this coordination, it was found that the carbonyl bond weakened to almost a single bond (bond order = 1.2).

No surface reconstruction occurred for binding at the 3c sites, but this occurred when the adsorption took place at higher coordination sites, which leads to the question whether the surface reconstruction is a requirement for adsorption or the nanotube itself is more stable than the bulklike structure, which represents perhaps a metastable local minimum on the $(MgO)_{12}$ potential energy surface. We therefore first determined the stable geometry of the cluster. The binding energies of the bulklike (unrelaxed) $(MgO)_{12}$ unit is −2420.7 kcal/mol, which changes to −2441.9 kcal/mol on geometry optimization, resulting in smaller Mg—O bond lengths and rounded edges. However, the most stable structure is found to be the MgO nanotube, having a binding energy of −2455.0 kcal/mol. Consequently, as it is

TABLE 1: Calculated Relative Energies (kcal/mol) for the Stationary Points on the Potential Energy Surface for the Reaction of Formaldehyde on the $(MgO)_{12}$ Surface

structure[a]	relative energy
3c Site	
$(MgO)_{12}$−formaldehyde (**1**)	−34.8
transition state (**2**)	−5.5
product (**3**)	−23.9
4c Site	
$(MgO)_{12}$−formaldehyde (**4**)	−18.0
transition state (**5**)	23.3
product (**6**)	−7.3

[a] Some of the structures are displayed in Figure 1.

more stable than even the relaxed bulklike cubic structure by 13.1 kcal/mol, all further calculations were carried out for adsorption at the $(MgO)_{12}$ nanotube, consisting of four stacked hexagonal $(MgO)_3$ rings. Moreover, the calculated energy barrier for the rearrangement of the cubic structure to the tube is only 3.4 kcal/mol. Indeed, mass spectral and collision-induced-fragmentation (CIF) studies on gas-phase sputtered MgO cluster ions,[56] and infrared resonance-enhanced multiphoton ionization spectroscopy,[57] show the predominance of $(MgO)_{3n}^+$ clusters for $n \leq 10$, indicating the presence of stacked hexagonal rings, as found in the present calculations. For larger values of n, however, the peaks were found to correspond to cubic bulklike clusters. Similar conclusions were obtained from theoretical calculations.[58]

The nanotube has a barrel-like structure. The interior Mg—O distances average 1.975 Å, while the outer ones are about 0.02 Å longer, i.e., 1.994 Å. These distances are much smaller than those in bulk Mg—O, 2.132 Å. Thus, the average length of the nanotube is 5.963 Å. The nanotube has only two kinds of coordinated sites, edge 3c and planar surface 4c sites, and all ions are on the surface. We first considered adsorption of formaldehyde (binding energy = −393.5 kcal/mol) at the former site. As found for the cubic crystal,[1] formaldehyde is initially adsorbed forming a four-membered ring with one MgO unit, involving interaction of the carbonyl oxygen with the magnesium ion and the carbon with the oxide ion, resulting in a formate-like structure. Taking the initially adsorbed structure as the reactant, we explored the minimum energy path for further reaction. This revealed heterolytic cleavage of a formaldehyde C—H bond, resulting in a hydride ion which, on combining with Mg^{2+}, gives an adsorbed $Mg—H^+$ and a formate ion involving a surface oxide.

Table 1 gives the calculated energies relative to the total energy of isolated formaldehyde and the $(MgO)_{12}$ nanotube for all points on the reaction surface. This table reveals that the reaction is endothermic ($\Delta H = 10.9$ kcal/mol) and the activation barrier is 29.3 kcal/mol. Although the barrier appears large, the energy required is compensated for by the high exothermicity (−34.8 kcal/mol) for the initial adsorption process. Figure 1 gives the structures of the reactant (**1**), transition state (**2**), and product (**3**). Thus, spontaneous dissociation is indicated, and the initial process in the adsorption of formaldehyde must be a heterolytic dissociation of a C—H bond, leading to adsorbed $[(MgH)^+(HCOO)^-]$.

We next investigated adsorption at the 4c coordination sites on the surface of the nanotube. On adsorption of formaldehyde with its carbon at a surface 4c oxide ion and its oxygen at a 4c magnesium ion, the 4c sites become trigonal bipyramid five-coordinate sites. We also investigated dissociative adsorption at this site, since the different geometry would result in a different initial distance of the formaldehyde hydrogens from magnesium ions. The calculations show that, in this case, one of the adsorbed formaldehyde hydrogens is transferred to an edge three-coordinate magnesium (see Figure 1). The transition state (**5**) has a four-center-like structure. As for the three-coordinate adsorption, the process is endothermic ($\Delta H = 10.7$ kcal/mol), and the barrier to this rearrangement is high (41.3 kcal/mol). In this case, too, the initial adsorption is exothermic (−18.0 kcal/ mol), but the energy evolved is not sufficient to carry the reaction over the activation barrier. One surface MgO unit is involved in this product (see Figure 1). However, it can be seen that the adsorption process itself is less exothermic and the barrier to rearrangement is also higher for adsorption at this higher coordinate site, although the enthalpy for the rearrangement is not affected by the change in coordination of the adsorption sites.

Table 2 gives the calculated partial charges on the atoms of the adsorbed formaldehyde molecule and the MgO unit at the site of adsorption. In both cases, it is clear that it is a hydride ion that shifts to the magnesium dication.

III.2. Adsorption and Dissociation of Acetaldehyde. We also considered the adsorption and decomposition of acetaldehyde, which has one of the formaldehyde hydrogens replaced by a methyl group, and thus the migrating hydrogen could be either the aldehyde hydrogen or a methyl hydrogen. For molecules bearing a methyl group adjacent to a carbonyl (e.g., acetic and thioacetic acids, acetone, acetaldehyde, and pyruvic acid), the methyl group assumes a conformation where one of the hydrogen atoms is synperiplanar with respect to the carbonyl oxygen. The higher stability of this conformation is due to more favorable $\pi(CH_3) \rightarrow \pi^*(C{=}O)$ group orbital interactions and hyperconjugation through the σ bond system.[59] The present calculations show that this conformation of acetaldehyde (−705.9 kcal/mol) is more stable than the anti structure by 0.9 kcal/mol.

Two orientations for adsorption of acetaldehyde on the MgO nanotube surface were considered: one in which the carbonyl oxygen is aligned over a magnesium ion, and the formaldehyde carbon is not involved in interaction with any oxide ion (**A**), and the second in which the carbonyl bond is tilted horizontally, as in formaldehyde, the carbonyl carbon forming a close contact with a surface oxide ion and the carbonyl oxygen interacting with a magnesium ion (**B**).

In the former case (**A**), it was found that the carbon−oxygen bond tilts horizontally, enabling one of the methyl hydrogens to come in close contact with a surface oxygen. The optimized O—H distance (1.97 Å) is short and is much smaller than the sum of the van der Waals radii of oxygen and hydrogen (2.72 Å), indicating that, in this mode of adsorption, there are interactions between the surface magnesium ion and carbonyl oxygen, and the surface oxide ion with a methyl proton (Figure 2). Since the methyl hydrogen is in close proximity to a surface oxide ion, it should be relatively easy for this to migrate to the surface. The transition state (**8**) and product (**9**) are also depicted in the figure. In this heterolytic cleavage of a C—H bond of the methyl group of acetaldehyde, the proton migrates to an edge 3c surface oxide ion, giving rise to an HO^- ion. The remaining $[OC(H){=}H_2]^-$ moiety combines with a surface Mg^{2+}, producing $Mg[OC(H){=}H_2]^+$. The reaction proceeds with low barrier (8.7 kcal/mol) and is exothermic ($\Delta H = -17.4$ kcal/mol). In the product (**9**), the surface Mg—O unit length increases to 3.35 Å from 2.12 Å in the initially adsorbed structure (**A**). The CH_2 carbon also has a close contact with a 3c Mg, the distance, 2.42 Å, being much smaller than the sum of Mg and C van der Waals radii (3.43 Å).

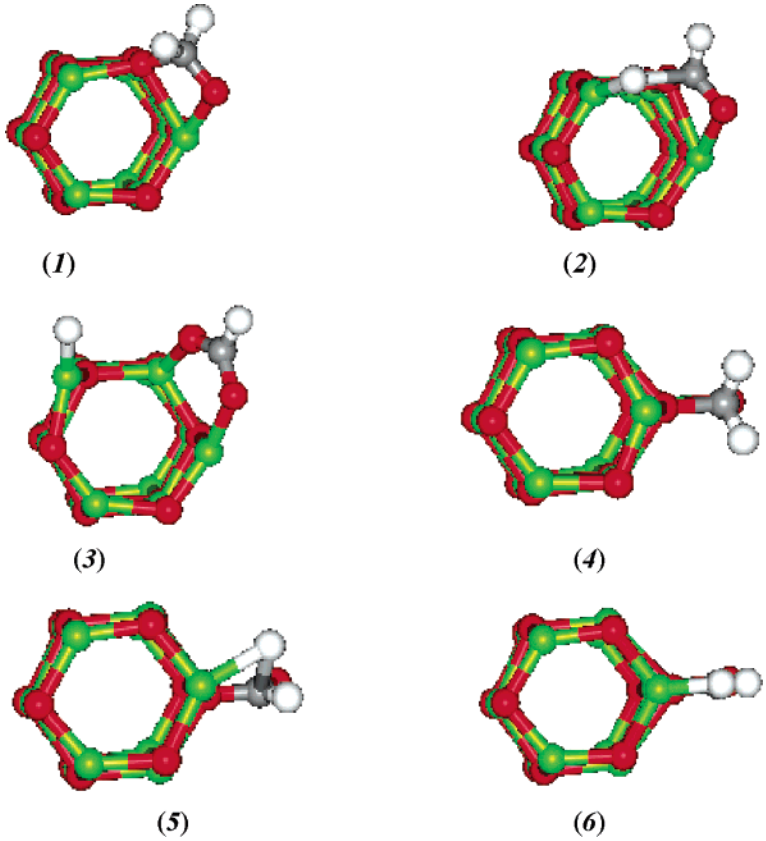

Figure 1. Optimized structures of the initially adsorbed structure (**1**), transition state (**2**), the product (**3**) of dissociation of formaldehyde at the 3c MgO site; the initial structure (**4**), transition state (**5**), and the product (**6**) of dissociation of formaldehyde at the 4c MgO site. Color code: Mg, green; O, red; C, gray; H, white.

TABLE 2: Calculated ESP-Fitted Charges on the Adsorbed Formaldehyde Moiety and the Surface Mg and O Atoms Involved in the Reaction

atom	adsorbed formaldehyde	transition state	product
	3c Site		
O	−0.728	−0.546	−0.503
C	0.283	0.357	0.171
H	0.091	0.144	0.150
H[a]	0.014	−0.470	−0.516
Mg	1.248	1.273	1.224
O	−1.043	−0.629	−0.356
Mg[b]	1.341	1.103	1.067
	4c Site		
O	−0.908	−0.766	−0.654
C	1.126	1.204	1.123
H	−0.159	−0.103	−0.112
H[a]	−0.159	−0.449	−0.512
Mg	1.286	1.246	1.199
O	−1.393	−1.431	−1.139
Mg[b]	1.269	1.246	1.108

[a] The migrating hydrogen. [b] Mg to which hydrogen migrates.

For adsorption in this mode at a pair of 3c corner sites, it was found that, not only does the methyl group tilt to bring a methyl hydrogen close to the 3c oxygen, but spontaneous dissociation of the C—H bond also occurs, leading to the formation of surface HO^- and $[MgOC(H)=H_2]^+$ moieties, according to the equation

$$CH_3CHO + Mg^{2+}O^{2-} \rightarrow Mg[OC(H)=H_2]^+ + HO^-$$

As for formaldehyde, initial adsorption at the nanotube surface in mode **B** yields a four-center-like structure (**10**), in which the surface $Mg_{4c}—O_{4c}$ bond is weakened, and a new $Mg_{4c}—O$ bond involving the carbonyl oxygen is formed (see Figure 2). The partial charges on the two oxygens are, respectively, −1.062

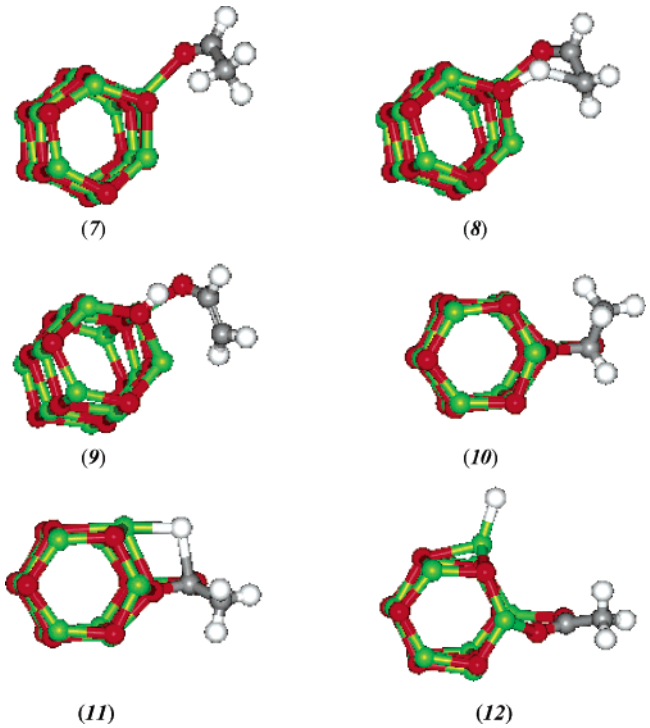

Figure 2. Optimized structures of the adsorption products of acetaldehyde: adsorbed acetaldehyde **A** (**7**), transition state (**8**), product (**9**) of dissociation of **A** by methyl C—H bond scission, adsorbed acetaldehyde **B** (**10**), and the transition state (**11**) and product (**12**) of aldehyde C—H dissociation.

TABLE 3: Calculated Relative Energies (kcal/mol) of Some Structures on the Potential Energy Surface for the Reaction of Acetaldehyde on the $(MgO)_{12}$ Surface

structure[a]	relative energy
adsorbed acetaldehyde (**A**) (**7**)	−8.6
transition state (**8**)	0.1
product (**9**)	−26.0
chemisorbed acetaldehyde (**B**) (**10**)	−10.6
transition state (**11**)	27.4
product (**12**)	8.6

[a] See Figure 2.

and −0.898, indicating the formation of an acetate-like species. The chemisorption process is itself exothermic ($\Delta H = -10.6$ kcal/mol). For the aldehyde hydrogen migration from this initially adsorbed acetaldehyde, the activation barrier (38.0 kcal/mol) and heat of reaction (19.2 kcal/mol) are similar to those found for formaldehyde. The transition state (**11**) is shown in Figure 2, and the product (**12**) is adsorbed acetate and MgH^+. The structures are similar to those observed for formaldehyde (Figure 1), and their energies are given in Table 3.

This shows that the aldehyde hydrogen prefers to migrate to a Lewis acid site, while the methyl hydrogens have a tendency to attach to the Lewis basic sites (oxide ions). The latter reaction is preferred, both on account of its lower energy of activation and higher stability of the product, while the former reaction is endothermic.

III.3. Adsorption and Dissociation of Acetone. The acetone−MgO system has been the subject of several infrared and temperature-programmed desorption studies,[60−62] and $^1H-^2H$ exchange experiments have been reported.[4] The effect of a keto−enol equilibrium for acetone has been shown[63] to significantly decrease the energy difference between the keto and enol tautomers. The stabilization of the enol tautomer would result in an increase of its surface concentration, accounting for the enhanced catalytic activity of the surface. We investigated the adsorption and dissociation of acetone on MgO nanotubes to see how the lower coordination sites would affect the equilibrium and direction of reaction.

In the gas phase, the keto tautomer (−1014.6 kcal/mol) is found to be more stable than the enol form by 14.7 kcal/mol. Since enolization on the planar surface has been reported,[62] we considered enol formation. In this case, there are only the methyl group C−H bonds that may dissociate. We first considered the migration of a methyl hydrogen to the carbonyl oxygen, resulting in adsorbed isopropenol. It has been reported[63] that, at the Hartree−Fock level, the adsorbed acetone enol tautomer is formed, and dissociation of isopropenol only occurs if the surface is relaxed. However, more refined calculations at the MP2 level of theory[62] led to the dissociation of isopropenol to the corresponding enolate and a proton bound to a surface oxygen atom. It may be noted that, in the above cited work,[62] a small $[MgO_5]^{8-}$ unit had been taken for the calculations performed using the embedded cluster method. Moreover, the Mg−O bond length had been fixed at 2.105 Å. We found that the initial adsorption is exothermic (−9.7 kcal/mol). O−H bond formation with a surface oxide takes place then. This step has an activation energy of 37.2 kcal/mol and is exothermic (−5.5 kcal/mol). The resulting structure (Figure 3) is partially dissociated isopropenol. The mechanism corroborates the mechanism proposed by us earlier following an FT-IR study of acetone adsorption on the MgO nanosurface.[2] Acetone is first adsorbed on the MgO surface, and then tautomerizes to give partly dissociated isopropenol. It may be noted that the keto−enol difference decreases from −14.7 to 5.5 kcal/mol; i.e., the enol form, which was less stable for free acetone, becomes more stable than the keto form after adsorption, as the proton is now simultaneously bonded to both the erstwhile carbonyl oxygen (1.717 Å) and the surface oxide (1.007 Å). The proton is positively charged (0.518), and the negative charge on the surface oxygen (−1.261) is higher than that calculated for the acetone oxygen (−0.549).

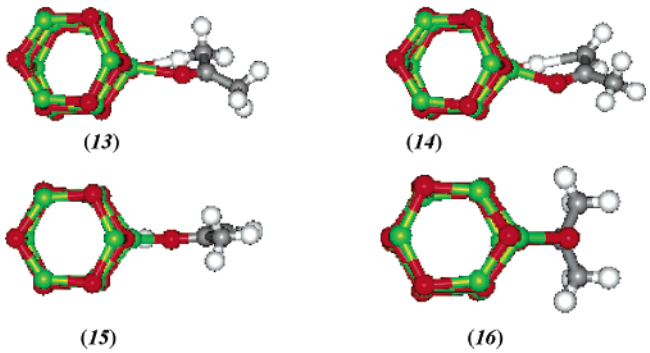

Figure 3. Optimized structures of adsorbed acetone on the $(MgO)_{12}$ nanotube (**13**), transition state (**14**) for formation of surface enolate (**15**), and the carboxylate (**16**).

III.4. Vibrational Spectra of Adsorbed Species. The adsorption of acetaldehyde and acetone on Aerogel prepared magnesium oxide nanocrystals (AP-MgO, surface area = 320−360 m^2/g) was earlier investigated[2] using FT-IR spectroscopy. In that study, nanocrystalline MgO had been obtained as a fine powder consisting of nanocrystals having an average 4 nm crystallite size.[64] In the present work, we have calculated the vibrational spectra of the species produced to aid the assignment of the spectra obtained.

For free acetaldehyde, the prominent peaks are expected to be the ones due to carbonyl stretching and the aldehyde C−H stretch. These were observed at 1761 and 2800 cm^{-1}, respectively.[2] The calculated values are 1812 and 2800 cm^{-1}, respectively, and these are the most intense bands, having calculated intensities of 172 and 136 km/mol, respectively. Less intense bands (intensity = ∼30 km/mol) at 1100 and 1328 cm^{-1} are also expected. It was further observed[2] that, on adsorption on MgO, a broad band appeared at higher frequency (∼2900 cm^{-1}) and the carbonyl band was gradually replaced by bands at lower frequency (1711 and 1566 cm^{-1}). Some close-lying bands were also observed in the 1000−1500 cm^{-1} region. According to the results reported in section III.2, the most feasible reactions on the nanosurface are expected to be methyl hydrogen migration resulting in (**9**), or formation of the carboxylate-like oxidized adsorption product (**10**). For (**9**), the important peaks in the 1000−4000 cm^{-1} region are expected to be 1349 cm^{-1} (C−O stretch + HCO bend, 110 km/mol), 1564 cm^{-1} (C=C stretch, 314 km/mol), and 2899 cm^{-1} (aldehyde C−H stretch, 134 km/mol). For (**10**), only two prominent bands are expected, 1164 cm^{-1} (C−O stretch, 139 km/mol) and 2823 cm^{-1} (aldehyde C−H stretch, 159 km/mol). If further reaction to (**12**) occurs, the spectrum is expected to be dominated by a very intense band at 1395 cm^{-1} (559 km/mol), which is a mixture of C−O stretch, HCO bend, and Mg−H stretch. Other bands are expected at 1406 cm^{-1} (Mg−H stretch, 109 km/mol) and 1544 cm^{-1} (C−O stretch, 367 km/mol). In the observed spectrum, the presence of a broad band at 2900 cm^{-1} seems to preclude the presence of (**12**), which is the only structure that lacks an aldehyde C−H band. Moreover, this structure has a higher energy than the other two structures. The calculated vibrational frequencies seem to favor (**9**), the product of methyl hydrogen dissociation, because of the presence

TABLE 4: Calculated Relative Energies (kcal/mol) of Some Structures on the Potential Energy Surface for the Reaction of Acetone on the $(MgO)_{12}$ Surface

structure[a]	relative energy
adsorbed acetone (**13**)	−9.7
transition State (**14**)	27.5
enolate (**15**)	−15.2
carboxylate-like structure (**16**)	18.7

[a] See Figure 3.

of the strong band at 1564 cm^{-1}. These observations support the present calculations, which predict that methyl hydrogen migration to a surface oxide is favored, as the corresponding reaction is exothermic and has the smallest energy of activation.

In the case of acetone, the presence of enolate species was also indicated by a DRIFT spectroscopic study of the acetone−MgO system.[62] The authors ascribed a new band at 1640 cm^{-1} to adsorbed enolic species. Our calculations with the larger MgO cluster and DFT level also confirm this. For acetone, the calculated carbonyl stretching band is at 1745 cm^{-1}. This compares well with the experimental value[62] of 1735 cm^{-1}. For the adsorbed enolate (**15**), the expected prominent bands in the >1000 cm^{-1} region are 1301 cm^{-1} (193 km/mol), 1348 cm^{-1} (143 km/mol), 1635 cm^{-1} (317 km/mol), and 3100 cm^{-1} (1062 km/mol). The first two contain varying degrees of CCO group stretching and symmetrical bending vibrations of the methyl group, as well as the HC═C bending mode. The band at 1635 cm^{-1} is due to C═C stretching, while the most prominent band at 3100 cm^{-1} is due to the hydroxyl stretching mode. The experimental spectrum[2] is dominated by bands at 1250, 1364, 1611, and 2955 cm^{-1}. The last band was incorrectly assigned to a C−H stretch (but is, in fact, due to the hydroxyl stretch, as it has high intensity, while the C−H stretching bands have lower intensities) and the band at 1611 cm^{-1} to the carbonyl stretch. In fact, the carbonyl bond weakens so much due to interaction with the surface that its vibration shifts to the 1300−1400 cm^{-1} region. Both the present calculations and our earlier work show the disappearance of the carbonyl stretching vibration at 1745 cm^{-1} after adsorption. However, the DRIFT spectrum of adsorbed acetone on bulk MgO[62] showed the presence of this band even after adsorption, and the authors interpreted this to indicate weak physisorption. This important difference shows that acetone is dissociatively adsorbed on nanosurfaces and only weakly adsorbed on bulk MgO. Moreover, while intense bands corresponding to carboxylate species have also been reported,[62] these were not found in the FT-IR spectrum of acetone adsorbed on AP-MgO. The present calculations reveal that the carboxylate species is much higher in energy as compared to the enolate (Table 4).

IV. Discussion

Before we state the main conclusions of this study, let us discuss the dependence of the results on various factors, such as choice of the nanoparticle size and shape, functional and basis set, and the possible limitations of the present study. Regarding the first, we had found[1] the $(MgO)_{12}$ cluster to be of the appropriate size to describe a small finite nanocluster. It may be argued that the small particle is susceptible to probably unphysical reconstruction on geometry optimization, which may have resulted in the tube becoming more stable than the cubic structure. However, it is gratifying to note that experimental observations[55−57] indicate the existence and stabilities of such stacked hexagonal rings, at least for small gas-phase clusters. Moreover, there have been recent reports on the synthesis and

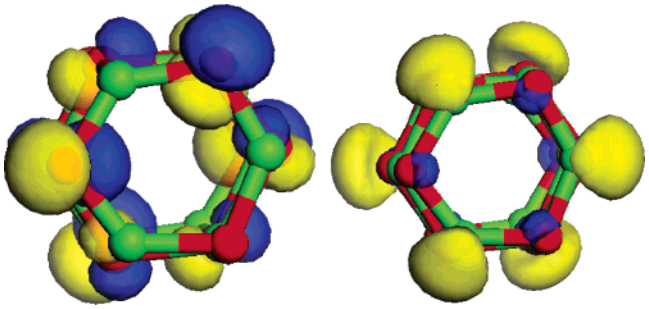

Figure 4. Isosurfaces (isovalue = 0.03 a.u.) of the HOMO and LUMO of the $(MgO)_{12}$ nanotube.

properties of MgO nanotube bundles,[65] preparation of single-walled carbon nanotube reinforced magnesia films,[66] as well as the application of Ga filled MgO nanotubes as nanothermometers.[67] Several different structures including nanorods,[68] nanobelts,[69] nanowires,[70] aligned crystalline nanoporous films,[71] three-dimensional nanostructures,[72] and fishbone fractal nanostructures[73] have been fabricated. These experimental and theoretical[74] studies have provided evidence for the existence and stabilities of MgO nanotubes, as found from our calculations.[1] Thus, the reconstruction of the nanosurface is not an artifact of the calculation method. Rather, small MgO clusters prefer the nanotube geometry over the bulklike structure, as evidenced from their mass spectra.[55−57] Since the cluster size taken in this study is within the range of preferred stacked ring structures, the theoretical results are in consonance with the experimental observations.

For small MgO clusters, the experimental[57] vibrational frequency is found at 640 cm^{-1}, and this matches with a strong resonance observed at 651 cm^{-1} in the high-resolution electron energy loss spectroscopy (HREELS) measurements on the solid surface.[75] The HREELS surface phonon spectra is assigned as the optically allowed motion of oxygen atoms stretching perpendicular to the surface. Our calculations indicate that the vibrational frequency for the perpendicular band of the nanotube is at 657 cm^{-1} (intensity = 1132 km/mol), and for the bulklike structure, the band is at 677 cm^{-1} (intensity = 705 km/mol). Another broad band was observed[57] at ∼455 cm^{-1}, but this band was found to be cluster-size dependent, getting blue-shifted and increasing in intensity with increasing cluster size. Both the structures show bands in this region, the tube showing a band at 452 cm^{-1} with an intensity of 125 km/mol, while the bulklike structure is expected to have vibrational bands at 463 cm^{-1} (intensity = 251 km/mol) and 470 cm^{-1} (128 km/mol). Again, the correspondence is slightly better for the nanotube structure than for the bulklike nanocluster.

As noted previously, the relaxation of the nanosurface is a requirement for chemisorption to take place, as keeping the nanosurface fixed at the rock salt geometry of the bulk does not lead to any interaction between the adsorbate and the nanosurface. Bulk MgO is known to be relatively inert, but its reactivity is enhanced in the nanoscale,[76] due to the different structure, leading to smaller coordination numbers of the metal oxide ions.

The next question concerns the choice of functional in the DFT calculations. For molecular systems, hybrid functionals[77] such as the popular B3LYP, which include a portion of exact Hartree−Fock (HF) exchange, yield excellent results. However, there is a problem of practicability. Even for finite band gap systems, where such calculations are feasible, the CPU time requirement is extremely high. There are also convergence problems of hybrid functionals, especially for small band gap

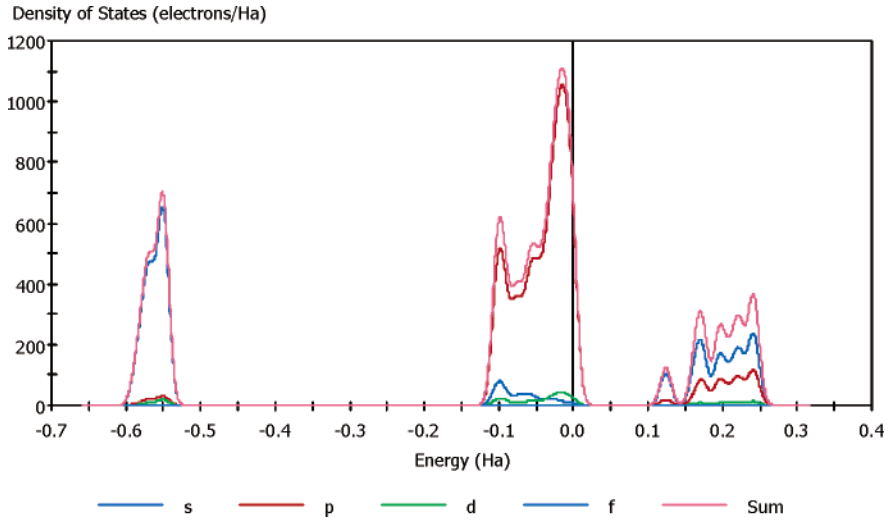

Figure 5. Density of states for the nanotube cluster.

systems. Moreover, the physical properties are not correctly predicted with these functionals.

Therefore, we are only left with a choice from among the nonhybrid density functionals. There is only limited experimental data concerning the adsorption of carbonyls on MgO nanosurfaces, and to our knowledge no directly comparable calculations on this system, so we must compare our results to calculations and experiments on other systems to assess the effects of different density functionals.[37,39,40] For a suite of simple molecules, the LDA was shown[78] to overbind by an average of 36.2 kcal/mol, while the addition of gradient corrections reduced this average error to 3.7 kcal/mol. Of the several GGA functionals available, PBE was chosen, as it is found to perform better[79] and is suited for both molecules and solids. Moreover, it does not contain empirically adjusted parameters and is known to be reliable for geometry optimization.[42,80]

However, a deficiency of all nonhybrid density functionals is their tendency to underestimate band gaps,[81] since the exchange potential is particularly important for its calculation. The mean average error for PBE is 1.13 eV[82] for a semiconductor set of 40 solids containing 13 group IIA−VI systems, six group IIB−VI systems, 17 group III−V systems, and four group IV systems, including a few systems with larger band gaps (diamond, BN, AlN, MgO, and MgS). For bulk MgO, the experimental value of the band gap is 7.22 eV.[8] The band gap problem for solids in DFT is closely related to the HOMO−LUMO (highest occupied molecular orbital−lowest unoccupied molecular orbital) gap problem for molecules. The magnitude of this gap is important, as the relative positions of the HOMO and LUMO of the surface and adsorbate determine the extent of their mutual interaction. Although the electron affinities and ionization potentials for atoms and molecules can now be determined with very high accuracy, the equivalent parameters are particularly unknown for the kind of system taken in the present study.

However, the band gap does not appear to be as important a factor as the local coordination of sites at which adsorption takes place in determining surface reactivity. As noted previously, the preferred geometry for this cluster is a tubular structure. The nanosurface becomes more stable than the rectangular bulklike cluster due to stabilization of the occupied levels. The isosurfaces of the HOMO and LUMO, shown in Figure 4, reveal that these comprise mainly the 2p orbitals of oxygen and 3s and 3p orbitals of Mg, respectively. The LUMO has a strong oxygen 3s component (see Figure 4) as well. This is the reason for the Mulliken populations being much lower than the formal ±2 charge states of the lattice.[1] The participation of the anion MOs in the LUMO has been reported previously.[84] We found that the LUMO is occupied by 0.01 e^-. The anion-centered nature of the HOMO means that its energy depends on the O−O distances, too. In the MgO nanotube, the average O−O distance of the edge oxygens is 4.45 Å, compared to two O−O distances of 2.96 Å and another two oxygens separated by 3.98 Å for the rectangular cluster. The smaller anion−anion repulsion in the nanotube stabilizes the HOMO, increasing the HOMO−LUMO gap. In spite of this increase, this structure is more reactive toward carbonyls, because of the decrease in the local coordination at the adsorption sites by increase in the distance of the ion from the oppositely charged ion below it.

For the sake of comparison, we also performed periodic boundary calculations to model solid clusters of the stacked-ring and cubelike structures, and obtained their electronic density of states. The clusters were positioned in large supercells of side 15 Å. This ensured that the distance between two clusters in neighboring cells is at least 9 Å, minimizing their mutual interaction. The *k*-point sampling was done by the use of the Monkhorst−Pack scheme.[85] Only a slight change in geometry of the stacked ring cluster resulted on geometry optimization. The central Mg−O bond distances increase to an average of 1.991 Å and the exterior ones to 2.016 Å. Thus, the inter-ring spacing increases, leading to a slight increase in the end-to-end distance to 6.023 from 5.963 Å. The relative stability of the nanotube with respect to the bulklike structure also increases to 25.7 kcal/mol.

The electronic density of states (DOS) for this periodic superstructure consisting of stacked rings is shown in Figure 5. The separation of bands is about 3.4 eV, which is slightly higher than that obtained for the bulklike cluster (3.1 eV). The DOS plots for the nanotube and cubelike structure are qualitatively similar. By analogy with other similar systems, it is expected that the band gap in nanocrystals is smaller (in contravention of the principles of quantum confinement) than the bulk, and the HOMO decreases in energy, while the LUMO goes up with size, to eventually evolve into the top of the valence and bottom of the conduction bands, respectively, of the bulk material. In ionic materials, the stabilization of the HOMO with size is expected on the basis of increase in Mulliken population, since the components of the electrostatic fields due to the individual ion charges increase with cluster size. In keeping with this, the

estimated gap (3.4 eV) for the stacked ring geometry of $(MgO)_{12}$ agrees with the fact that the band gap, calculated at the same level, for bulk MgO, is 4.8 eV. When the calculations for adsorption of acetaldehyde on MgO nanotube clusters were repeated for the supercell, the same mechanism for acetaldehyde methyl dissociation was found to prevail, but the exothermicity of the reaction decreased from 17.4 to 15.8 kcal/mol.

Next, we need to carefully assess the numerical accuracy of our results. The largest source of uncertainty in an ab initio calculation is basis set incompleteness, including the related issue of basis set superposition error (BSSE). The present method does not permit us to estimate BSSE by the counterpoise method, since we cannot place extra basis functions at points where there are no atoms. Again, we rely on previous calculations for our assessment of BSSE. As stated in section II, DMol[3] uses numerical functions that are far more complete than traditional Gaussian functions, and therefore, we expect BSSE contribution to be small. Furthermore, according to Delley,[36] molecules can be dissociated exactly into their constituent atoms (within the DFT context) thereby minimizing or even eliminating basis set superposition error (BSSE). Hence, it should be possible to obtain an accurate description, even for weak bonds. The BSSE for the DNP basis set is found to be comparable with that for the much larger Gaussian basis set (6-311+G-(3df,2pd)), and is hence low. In a recent paper,[86] DNP was compared with various Gaussian basis sets for hydrogen-bonded systems, and it was concluded that the upper limit of the mean error for the DNP basis set employed in conjunction with the PBE functional, due to neglect of BSSE, is less than 1 kcal/mol. This is much smaller than the energy quantities involved in the various processes studied here. We may therefore surmise that the errors due to band gap underestimation and BSSE are small enough to leave our qualitative conclusions unchanged.

V. Conclusions

The most important conclusions from the present calculations are that strong chemisorptions of carbonyl compounds occur on metal oxide nanosurfaces represented by four hexagonal stacked ring structures, corresponding to $(MgO)_{12}$. Dissociation of the carbonyl compound takes place relatively easily on these MgO nanotubes, as all the ions are at the surface and have low coordination numbers. The greater stability found for these nanotubes for small clusters agrees with several mass spectral and IR studies on gas-phase clusters, as well as previous theoretical calculations. The stabilities of nanotubes vis-à-vis bulklike cubic structures are due to the larger O—O distances in the former, minimizing the mutual repulsion of the oxide anions.

In the case of aldehydes, the aldehyde hydrogen migrates to the magnesium ion; alkyl hydrogens prefer the basic oxygen ions. The former is a case of hydride migration, while the latter is proton migration, and is preferred both in terms of the stability of the final product and the lower activation barrier to its formation. Comparison of the calculated vibrational spectrum with the observed FT-IR spectrum of acetaldehyde adsorbed on MgO nanoclusters confirms that this is the final product.

For acetone, it is found that enolization takes place, and the resulting enol tautomer is strongly bound to the surface through the oxygen of the enol hydroxyl (on Mg^{2+}) and the hydroxyl hydrogen (on O^{2-}), resulting in a reversal of the keto−enol equilibrium in favor of the enol form.

The important result is that dissociation is spontaneous at the edges of the nanotubes. Since small particles have a greater proportion of edges and have the ability to take on interesting shapes because of their small size, they can be profitably utilized to remove toxic gases from the environment, particularly for the improvement of indoor air quality. The resulting products are strongly bound to the nanosurface and are not easily removed. Moreover, the Mg—O bond ruptures at the site of adsorption, exposing new surfaces for further adsorption.

In particular, the present calculations have helped unambiguously assign the FT-IR spectra of acetaldehyde and acetone adsorbed on MgO nanosurfaces.

Acknowledgment. K.J.K. gratefully acknowledges the Army Research Office and the National Science Foundation.

References and Notes

(1) Kakkar, R.; Kapoor, P. N.; Klabunde, K. J. *J. Phys. Chem. B* **2004**, *108*, 18140.
(2) Khaleel, A.; Kapoor, P. N.; Klabunde, K. J. *Nanostruct. Mater.* **1999**, *11*, 459.
(3) Kapoor, P. N.; Bhagi, A. K.; Mulukutla, R. S.; Klabunde, K. J. *Dekker Encyclopedia of Nanoscience & Technology*; Marcel Dekker Inc.: New York, 2004.
(4) Zhang, G.; Hattori, H.; Tanabe, K. *Appl. Catal., A* **1988**, *36*, 189.
(5) Knözinger, E.; Jacob, K.-H.; Hofmann, P. *J. Chem. Soc., Faraday Trans.* **1993**, *89*, 1101.
(6) Shido, T.; Asakura, K.; Iwasawa, Y. *J. Chem. Soc., Faraday Trans. 1* **1989**, *85*, 441.
(7) Shido, T.; Asakura, K.; Iwasawa, Y. *J. Catal.* **1990**, *122*, 55.
(8) Driscoll, D. J.; Martir, W.; Wang, J.-X.; Lunsford, J. H. *J. Am. Chem. Soc.* **1985**, *107*, 58.
(9) Ito, T.; Lunsford, J. H. *Nature* **1985**, *314*, 721.
(10) Ito, T.; Wang, J.; Lin, C. H.; Lunsford, J. H. *J. Am. Chem. Soc.* **1985**, *107*, 5062.
(11) Hattori, H.; Tanaka, Y.; Tanabe, K. *J. Am. Chem. Soc.* **1976**, *98*, 4652.
(12) Boudart, M.; Delbouille, A.; Derouane, E. G.; Indovina, V.; Walters, A. B. *J. Am. Chem. Soc.* **1972**, *94*, 6622.
(13) Kunz, A. B.; Guse, M. P. *Chem. Phys. Lett.* **1977**, *45*, 18.
(14) Coluccia, S.; Boccuzzi, F.; Ghiotti, G.; Mirra, C. *Z. Phys. Chem.* **1980**, *121*, 141.
(15) Coluccia, S.; Boccuzzi, F.; Ghiotti, G.; Morterra, C. *J. Chem. Soc., Faraday Trans. 1* **1982**, *78*, 2111.
(16) Ito, T.; Sekino, T.; Moriai, N.; Tokuda, T. *J. Chem. Soc., Faraday Trans. 1* **1981**, *77*, 2181.
(17) Ito, T.; Kuramoto, M.; Yoshioka, M.; Tokuda, T. *J. Phys. Chem.* **1983**, *87*, 4411.
(18) Ito, T.; Murakami, T.; Tokuda, T. *J. Chem. Soc., Faraday Trans. 1* **1983**, *79*, 913.
(19) Ferrari, A. M.; Huber, S.; Knözinger, H.; Neyman, K. M.; Rösch, N. *J. Chem. Phys. B* **1998**, *102*, 4548.
(20) Anchell, J. L.; Morokuma, K.; Hess, A. C. *J. Chem. Phys.* **1993**, *99*, 6004.
(21) Kobayashi, H.; Salalahub, D. R.; Ito, T. *J. Phys. Chem.* **1994**, *98*, 5487.
(22) Shluger, A. L.; Gale, J. D.; Catlow, C. R. A. *J. Phys. Chem.* **1992**, *96*, 10389.
(23) Duński, H.; Jóźwiak, W. K.; Sugier, H. *J. Catal.* **1994**, *146*, 166.
(24) Knözinger, E.; Jacob, K.-H.; Singh, S.; Hofmann, P. *Surf. Sci.* **1993**, *290*, 388.
(25) Colbourn, E. A. *Surf. Sci. Rep.* **1992**, *15*, 281.
(26) Recio, J. M.; Pandey, R.; Ayuela, A.; Kunz, A. B. *J. Chem. Phys.* **1993**, *98*, 4783.
(27) Garrone, E.; Zecchina, A.; Stone, F. S. *Philos. Mag. B* **1980**, *42*, 683.
(28) Zecchina, A.; Lofthouse, M. G.; Stone, F. S. *J. Chem. Soc., Faraday Trans. 1* **1975**, *71*, 1476.
(29) Kobayashi, H.; Yamaguchi, M.; Ito, T. *J. Phys. Chem.* **1990**, *94*, 7206.
(30) Delley, B. *J. Chem. Phys.* **1990**, *92*, 508.
(31) Delley, B. *J. Chem. Phys.* **1991**, *94*, 7245.
(32) Delley, B. *J. Phys. Chem.* **1996**, *100*, 6107.
(33) Delley, B. *J. Chem. Phys.* **2000**, *113*, 7756.
(34) Matsuzawa, N.; Seto, J.; Dixon, D. A. *J. Phys. Chem. A* **1997**, *101*, 9391.
(35) Delley, B. *Phys. Rev. B* **2002**, *66*, 155125/1.
(36) Baker, J.; Kessi, A.; Delley, B. *J. Chem. Phys.* **1996**, *105*, 192.
(37) White, J. A.; Bird, D. M. *Phys. Rev. B* **1994**, *50*, 4954.
(38) Perdew, J. P.; Burke, K.; Ernzerhof, M. *Phys. Rev. Lett.* **1996**, *77*, 3865.

(39) van Santen, R. A.; Neurock, M. *Catal. Rev.—Sci. Eng.* **1995**, *37*, 557.
(40) Ziegler, T. *Chem. Rev.* **1991**, *91*, 651.
(41) Branda, M. M.; Belelli, P. G.; Ferullo, R. M.; Castellani, N. J. *Catal. Today* **2003**, *85*, 153.
(42) Kakkar, R.; Grover, R.; Gahlot, P. *Polyhedron* **2006**, *25*, 759.
(43) Singh, C. U.; Kollman, P. A. *J. Comput. Chem.* **1984**, *5*, 129.
(44) Le Page, J. F. *Catalyse de Contact*; Technip: Paris, 1978; p 385.
(45) Forzatti, P.; Tronconi, E.; Busca, G.; Tittarelli, P. *Catal. Today* **1987**, *1*, 209.
(46) Ai, M. *J. Catal.* **1983**, *83*, 141.
(47) Cant, N. W.; Tonner, S. P.; Trimm, D. L.; Wainwright, M. S. *J. Catal.* **1985**, *91*, 197.
(48) Klier, K. *Adv. Catal.* **1982**, *31*, 243.
(49) Mazanec, T. *J. Catal.* **1986**, *98*. 115.
(50) Biloen, P.; Sachtler, W. M. H. *Adv. Catal.* **1981**, *30*, 165.
(51) Busca, G.; Lamotte, J.; Lavalley, J-C.; Lorenzelli, V. *J. Am. Chem. Soc.* **1987**, *109*, 5197.
(52) Edwards, J. F.; Schrader, G. L. *J. Phys. Chem.* **1985**, *89*, 782.
(53) He, M. Y.; Ekerdt, J. G. *J. Catal.* **1984**, *90*, 17.
(54) Lavalley, J-C.; Lamotte, J.; Busca, G.; Lorenzelli, V. *J. Chem. Soc., Chem. Commun.* **1985**, 1006.
(55) Wang, G. W.; Hattori, H. *J. Chem. Soc., Faraday Trans. 1* **1984**, *80*, 1039.
(56) Saunders, W. A. *Phys. Rev. B* **1988**, *37*, 6583. Saunders, W. A. *Z. Phys. D* **1989**, *12*, 601.
(57) van Heijnsbergen, D.; von Helden, G.; Meijer, G.; Duncan, M. A. *J. Chem. Phys.* **2002**, *116* 2400−2406 and references therein.
(58) Wilson, M. *J. Phys. Chem. B* **1997**, *101*, 4917.
(59) Kakkar, R.; Pathak, M., Radhika, N. P. *Org. Biomol. Chem.* **2006**, *4*, 886.
(60) Lercher, J. A.; Noller, H.; Ritter, G. *J. Chem. Soc., Faraday Trans. 1* **1981**, *77*, 621.
(61) Miyata, H.; Toda, Y.; Kubokawa, Y. *J. Catal.* **1974**, *32*, 155.
(62) Sanz, J. F.; Oviedo, J.; Márquez, A.; Odriozola, J. A.; Montes, M. *Angew. Chem., Int. Ed.* **1999**, *38*, 506.
(63) Oviedo, J.; Sanz, J. F. *Surf. Sci.* **1998**, *397*, 23.
(64) Richards, R.; Li, W.; Decker, S.; Davidson, C.; Koper, O.; Zaikovski, V.; Volodin, A.; Rieker, T.; Klabunde, K. J. *J. Am. Chem. Soc.* **2000**, *122*, 4921.
(65) Yang, O.; Sha, J.; Wang, L.; Wang, Y.; Ma, X.; Wang, J.; Yang, D. *Nanotechnology* **2004**, *15*, 1004.
(66) Du, C.; Pan, N. *Nanotechnology* **2004**, *15*, 227.
(67) Li, Y. B.; Bando, Y.; Golberg, D.; Liu, Z. W. *Appl. Phys. Lett.* **2003**, *83*, 999.
(68) Yang, P.; Lieber C. M. *Science* **1996**, *273*, 1836; *J. Mater. Res.* **1997**, *12*, 2981.
(69) Bando, L. Y.; Sato, Y. T. *Chem. Phys. Lett.***2002**, *81*, 757. Ma, R.; Bando, Y. *Chem. Phys. Lett.* **2003**, *370*, 770 .
(70) Yin, Y.; Zhang, G.; Xia, Y. *Adv. Funct. Mater.* **2002**, *12*, 293.
(71) Dohnalek, Z.; Kimmel, G. A.; Mccready, D. E.; Young, S. J.; Dohnalkova, A.; Smith, R. G.; Kay, B. D. *J. Phys. Chem. B* **2002**, *106*, 3526.
(72) Klug, K. L.; Dravid, V. P. *Appl. Phys. Lett.* **2002**, *81*, 1687.
(73) Zhu, Y. Q.; Hsu, W. K.; Zhou, W. Z.; Terrones, M.; Kroto, H. W.; Walton, D, R. M. *Chem. Phys. Lett.* **2001**, *347*, 337.
(74) Bilalbegovic, G. *Phys. Rev. B* **2004**, *70*, 045407 and references therein.
(75) Henrich, V. E.; Cox, P. A. *The Surface Science of Metal Oxides*; Cambridge University Press: Cambridge, MA, 1994. Cox, P. A.; Williams, A. A. *J. Electron Spectrosc. Relat. Phenom.* **1986**, *39*, 45.
(76) Wagner, G. W.; Bartram, P. W.; Koper, O.; Klabunde, K. J. *J. Phys. Chem. B* **1999**, *103*, 3225.
(77) Becke, A. D. *J. Chem. Phys.* **1993**, *98* 1372.
(78) Becke, A. D. *J. Chem. Phys.* **1992**, *96*, 2155.
(79) Mortensen, J. J.; Kaasbjerg, K.; Frederiksen, S. L.; Nørskov, J. K.; Sethna, J. P.; Jacobsen, K. W. *Phys. Rev. Lett.* **2005**, *95*, 216401.
(80) Perdew, J. P.; Burke, K.; Ernzerhof, M. *Phys. Rev. Lett.* **1998**, *80*, 891.
(81) Perdew, J. P. *Int. J. Quantum Chem.* **1986**, *30*, 451.
(82) Heyd, J.; Peralta, J. E.; Scuseria, G. E. *J. Chem. Phys.* **2005**, *123*, 174101.
(83) Rafferty, B.; Brown, L. M. *Phys. Rev. B* **1998**, *58*, 10326.
(84) de Boer, P. K.; de Groot, R. A. *J. Phys.: Condens. Matter* **1998**, *10*, 10241.
(85) Monkhorst, H. J.; Pack, J. D. *Phys. Rev. B* **1976**, *13*, 5188.
(86) Benedek, N. A.; Snook, I. K.; Latham, K.; Yarovsky, I. *J. Chem. Phys.* **2005**, *122*, 144102.